A heat-powered ejector chiller working with low-GWP fluid R1233zd(E) (Part2: Numerical analysis)

A heat-powered ejector chiller working with low-GWP fluid R1233zd(E) (Part2: Numerical analysis)

Jafar Mahmoudian, Federico Mazzelli, Andrea Rocchetti, Adriano Milazzo* adriano.milazzo@unifi.it

DIEF- Department of Industrial Engineering, University of Florence, via S. Marta, 3, 50139 Florence, Italy

*Corresponding author.

Abstract

This paper numerically investigates the performance of a high capacity, industrial ejector chiller working with the non-flammable, low GWP refrigerant R1233zd(E). The test procedures adopted to acquire the experimental data are explained in part 1 of this work. Different turbulence models were examined in order to accurately predict the ejector off-design transition and critical pressure. A peculiar difference has been noticed between the numerical results obtained when initializing the CFD simulation from the solution of a case with lower or higher condenser pressure. This difference may partly explain the difficulties in the accurate predictions of the critical conditions reported by this and other works in the literature. A detailed discussion is presented on the nature and possible cause of this phenomenon, which is identified as typical of non-linear fluid dynamics.

Keywords: Ejector chiller; R1233zd(E); CFD; Retrofitting; Hysteresis

Nomenclature

latin

h Specific enthalpy, kJ kg^{-1}
K_a Arithmetic average roughness height
K_s Sand grain roughness height
K^+ Non-dimensional roughness height
$\dot{m}$ Mass flow rate, kg s^{-1}
P Pressure, bar
$\dot{Q}$ Heat flux, W
T Temperature,°C
u* Friction velocity, m s^{-1}
$\dot{W}$ Shaft power, W
Y^+ Non-dimensional wall distance

Greek

ε Rate of turbulence dissipation, m^2 s^{-3}
k Turbulent kinetic energy, m^2 s^{-2}
ρ Density, kg m^{-3}
τ Shear stress, Pa
ω Specific dissipation rate, s^{-1}

Subscripts

C Condenser
E Evaporator
EXP Experimental
G Generator
m Motive, primary
s Suction, secondary
sat Saturation

Acronyms

CFD Computational Fluid Dynamics
COP Coefficient of Performance
EOS Equation of State
ER Entrainment Ratio
GWP Global Warming Potential
MUSCL Monotonic Upwind Scheme for Conservation Laws
SST Shear Stress Transport

1 Introduction

The birth of the fourth generation of synthetic refrigerants was pushed by attention to global warming set forth by the Kyoto Protocol and by the newly enforced EU "F-gas" directive (European Commission 2017), which sets binding targets for greenhouse gas emissions. Many studies and review papers investigating the properties of these new refrigerants, termed Hydro-Fluoro-Olefins (HFOs) and featuring very low GWP, are available (Calm, 2008, Calm and Hourahan, 2011). ~~Reference~~ Fang et al. (2017) presents a CFD analysis of the behaviour of two HFOs as replacements for R134a in an ejector heat-driven refrigeration cycle. A thermodynamic comparison involving various fluids including HFOs was presented in ~~(~~Milazzo and Rocchetti (2015), highlighting the good performance of R1233zd(E). Among many options, R1233zd(E) has been proposed as the drop-in refrigerant for the hydrofluorocarbon R245fa also in ~~(~~Yang et al. (2019) and ~~(~~Eyerer et al. (2019). Recently, preliminary experimental and numerical investigations were carried out in our lab to test the performance of this new refrigerant inside our ejector refrigeration system (Mahmoudian et al., 2019). The present work represents the prosecution of those investigations, yielding additional experimental results, presented in part 1 of this paper, and a CFD analysis based on these results, presented in this second part.

When considering the specific field of ejector refrigeration, CFD modeling has a relatively short history. The review paper by ~~Matsuo et al. (1999) (~~Matsuo et al. (1999) cited pioneering papers modeling shock trains like ~~Carrol et al. (1993) (~~Carroll et al. (1993) and ~~Yamane et al. (1995) (~~Yamane et al. (1995), although these works were not specific to ejector applications. Ejector computational investigations gathered more importance in the last decade, thanks to improved computational resources and the advent of advanced CFD software. Authors have focused their studies on the analysis of several numerical aspects among which turbulence models and 2D–3D approximations had a central role.

~~Pianthong et al. (~~Pianthong et al. (2007) showed that there is no remarkable difference in wall pressure distribution along the ejector between the 2D and 3D approximation. ~~Mazzelli et al. (~~Mazzelli et al. (2015) found good agreement for an air-operated ejector, across all 2D and 3D models at on-design conditions. Automatically adapted grids have also been explored in many research articles (Al-Ansary and Jeter, 2004, Desevaux and Aeschbacher, 2002, Zhu and Jiang, 2014b) in order to find a compromise between simulation accuracy and computational cost.

In terms of turbulence modeling selection, ~~Bartosiewicz et al. (~~Bartosiewicz et al. (2003, Bartosiewicz et al., 2005) made a deep study to examine the effect of turbulence model by studying six models, ($k\varepsilon$, $k\varepsilon$-RNG-, $k\varepsilon$-Realizable, RSM, $k\omega$, $k\omega$-SST) applied to an air supersonic ejector. They proved that $k\varepsilon$-RNG and $k\omega$-SST are the best in predicting pressure variations, while the $k\omega$-SST model was better in predicting the mixing length of the motive jet. Following this work, they used the same turbulence models to evaluate the ER with R142b and found large prediction

differences, especially in off-design operations (Bartosiewicz et al., 2006). Further works focusing on ejectors operating under different conditions found that the $k\varepsilon$ and $k\omega$-SST gave the best performance compared to other models (García del Valle et al., 2015, Croquer et al., 2016). Recent reviews on ejector CFD studies are provided by ~~(~~Aidoun et al. (2019), Aidoun et al. (2019) and ~~(~~Grazzini et al. (2018).

Despite the vast plethora of ejector studies, aspects related to starting/unstarting problems and hysteresis inside ejectors have been less analyzed in the literature. Here we use the word "hysteresis" as the dependence of the state of a system on its history, i.e. the occurrence of different values of one variable depending on the direction of change of another variable. In particular, ~~Kim and Kwon (~~Kim and Kwon (2006) are among the few who showed the presence of hysteresis in their performance curves and stated that this behavior happened when the mixing chamber was longer than a certain critical length. They also reported that starting (unstarting) of the ejector occurs when the stagnation pressure of the primary flow is noticeably greater (lower) than a specific starting pressure (in turn, this starting pressure is proportional to the length of the mixing chamber). Once the ejector enters the supersonic operation mode, the primary flow pressure can be lowered to a value slightly higher than the unstarting pressure (Kim and Kwon, 2008).

The description of these phenomena is very similar to what occurs in supersonic and hypersonic wind tunnels, which suffer from the "start/unstart" issue caused by the presence of two subsequent choking sections (i.e., throats). This issue has been known since the very beginning of high-speed flow research (see for instance the work of ~~Kantrowitz and Donaldson (~~Kantrowitz and Donaldson (1945), or ~~Pope and Goin (~~Pope and Goin (1965) for a more specific reference on wind tunnel testing). Today, active research in this subject is carried out in the context of supersonic and hypersonic flight and is related to the catastrophic unstarting event of super/hypersonic inlet ducts (Chang et al., 2017). In this context, the starting/unstarting of the intake (also known as unstart/restart problem) has been recognized as a form of aerodynamic hysteresis (Van Wie et al., 1996).

Aerodynamic hysteresis has been experimentally identified and studied in various types of flow involving subsonic, transonic or supersonic regimes, with or without the presence of shocks or separation regions (Guzhavin and Korobov, 1984, Dan'kov et al., 2006, Shimshi et al., 2009). The most renowned and investigated case is related to airfoil stall (Mueller, 1985, Mittal and Saxena, 2000, Liaw and Abed, 1996). Despite the number of studies, a solid theoretical framework has been lacking for a long period: Guzhavin and Korobov report in 1988 the lack of theoretical explanations for the origin of this phenomenon (Guzhavin and Korobov, 1984). However, in the same period, pioneering works on aerodynamic bifurcations in fluid-dynamics were beginning to appear. For instance, ~~Tobak and Chapman (~~Tobak and Chapman (1985) were among the first to introduce the analogy between aerodynamic hysteresis and the (at that time new) theory of non-linear dynamic systems. Now, this field of study is well-established (see the book of ~~Holmes et al. (~~Holmes et al. (2012) for a comprehensive introduction) and it is more common to find papers that associate the concept of aerodynamics hysteresis with terms like bifurcations, multistability, metastable states, catastrophe theory, flow memory, spontaneous rearrangement, etc. (see for instance (Tao et al., 2009, Cui et al., 2011)).

The objective of this work is twofold. First, extend the experimental results obtained in part 1 by making use of compressible CFD analyses, which allow studying internal details of the ejector that are precluded from the experimental investigation. Second, to discuss some CFD results that seem to show the presence of hysteresis within the ejector internal flow field (e.g., persistent recirculation regions), as well as in its characteristic curve (hysteresis loops). We anticipate that such a presence was not clearly evident in the experimental tests carried out in our lab. Therefore, a discussion of this discrepancy is also given, in order to clarify the possible reasons and to understand whether CFD results should or should not be considered legitimate.

2 Numerical modeling

In the present work, simulations are performed using the commercial CFD package ANSYS FLUENT v19.2 that is based on a finite volume approach. The numerical model solves for the standard Navier-Stokes equations for compressible flows. Spatial discretization of both the conservation and turbulence equations is third-order accurate using the MUSCL scheme. Due to the high Mach numbers in the flow field, a density-based implicit solver is used (ANSYS Inc 2018). The convergence of the solution is defined by an error in the mass flow imbalance below 10^{-5} kg s^{-1} and calculations are stopped when all residuals are stable. Boundary conditions are provided as total pressure and static temperatures at inlets, static pressure at the outlet. Walls are assumed to be adiabatic. Based on successful

implementations reported in the literature (Menter et al., 2003, Bartosiewicz et al., 2005) and (Bartosiewicz et al., 2006), kω SST turbulence model is selected for all simulations.

All calculations are performed by accounting for real gas properties of the refrigerant using a 3rd order algebraic Peng-Robinson equation of state (EOS). The accuracy of this equation was compared against the NIST Refprop database. The results showed a very close agreement between the two solutions (differences were practically non-detectable inside the various contours, for instance, see Fig. 11 in (Mazzelli and Milazzo, 2015)), but computational speed was significantly increased in case of the algebraic EOS.

In order to limit computational resources, the fluid domain is selected to be 2D-axisymmetric. The specific dimensions of the ejector being investigated are reported in part 1 (or in (Mazzelli and Milazzo, 2015)), which also describes in detail the experimental setup and procedure used during the test campaign.

Fig. 1 shows the numerical grid together with detail in the proximity of the primary nozzle trailing edge and primary nozzle throat. Grid dependence was checked for the same geometry in (Mazzelli and Milazzo (2015) by comparing the results of three grids (Fig. 1), with grid refinement ratio of around 2 (the grids had approximately 40 000, 80 000 and 150 000 quadrilateral cells). The analysis showed that the 80 000 cells grid is the best trade-off in terms of accuracy and computational cost and the maximum error in the prediction of the mass flow rate was < 0.1% than the finest grid value. Moreover, the analysis of the local trends of Mach and pressure along the ejector revealed negligible discrepancies between the various grids (more details on grid convergence can be found in (Mazzelli and Milazzo, 2015)).

alt-text: Fig. 1

~~Figure~~Fig. 1

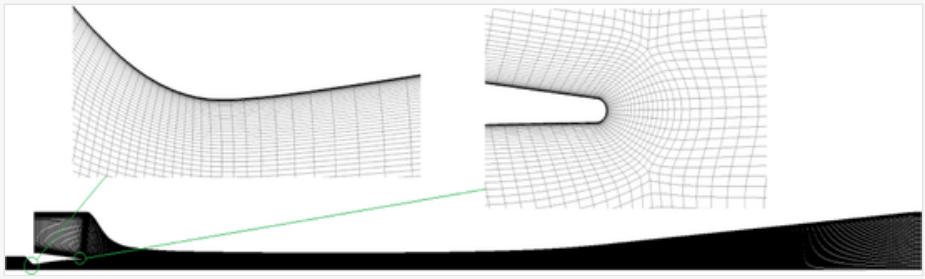

Numerical grid in the diffuser with the proximity of the primary nozzle trailing edge and primary nozzle throat.

The grid is designed to have y+ values always less than 1 when the surface is smooth. This choice enables obtaining better agreement with experiments, especially in the problems related to drag coefficient estimation and conjugate heat transfer (Brezgin et al., 2017) or when strong pressure gradients occur due to high back pressure and the presence of shocks.

When roughness is accounted for, ANSYS Fluent virtually shifts the wall by a quantity that is proportional to a non-dimensional roughness height:

$$Y^+ = Y^+ + K_s^+/2$$

Where K+ is the non-dimensional roughness height given by:

$$K_s^+ = \frac{\rho K_s u^*}{\mu}$$

Where ρ is the density, μ is the molecular viscosity, $u^* = \sqrt{\tau/\rho}$ is the friction velocity, τ is the shear stress and K_s is the physical roughness height (i.e., the diameter of the spherical sand-grain).

As a result of this shifting, the Y^+ quantity always remains larger by a halved height of the dimensionless sand-grain roughness height. This allows avoiding the singularity that occurs in the logarithmic velocity profile when the mesh is very fine and the wall is rough (a detailed analysis on the effect of surface roughness is provided by ~~Brezgin et al. (~~ Brezgin et al. (2017). The result is that fine meshes can be handled correctly even with rough wall conditions.

In summary, the numerical analysis is based on the following assumptions:

- 2D-axisymmetric domain
- Steady-state solution of the governing equations
- Adiabatic walls
- Surface roughness included (as explained in the next section)

3 Results and discussion

3.1 CFD simulation

For clarity, Fig. 2 reports the experimental supersonic ejector performance curve at constant generator temperature already shown in part 1. In the figure, the Coefficient Of Performance (COP) is defined as follows:

$$COP = \frac{\dot{Q}_E}{\dot{Q}_G + \dot{W}_{pump}} = \mathrm{ER}\frac{\Delta h_E}{(\Delta h_G + \Delta h_{pump})}$$

alt-text: Fig. 2

~~Figure~~Fig. 2

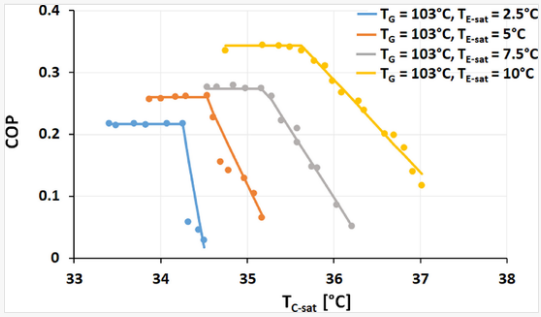

Experimental COP of the chiller in different conditions.

Where ER is the Entrainment Ratio:

$$ER = \frac{\dot{m}_s}{\dot{m}_m}$$

Among the various experimental conditions, the highest evaporator temperature ($T_{E\text{-}sat}$ = 10°C), which has the maximum COP at around 0.35 and critical temperature over 35.5°C, was chosen as the reference working condition for the setup of the CFD scheme. This choice was made because the experiments were most stable in this condition. Partly, this may be due to the fact that the off-design trend is less steep compared to other curves, which makes this condition less prone to instabilities and more appealing for the setup of the CFD.

The setup of the CFD scheme was done by analysing different computational models and comparing them against the selected experimental curve. The best model was then maintained for comparison with other experimental results.

Fig. 3 shows the comparison between experimental ER and mass flow rates and the corresponding CFD values calculated with different turbulence models and wall roughness.

alt-text: Fig. 3

~~Figure~~Fig. 3

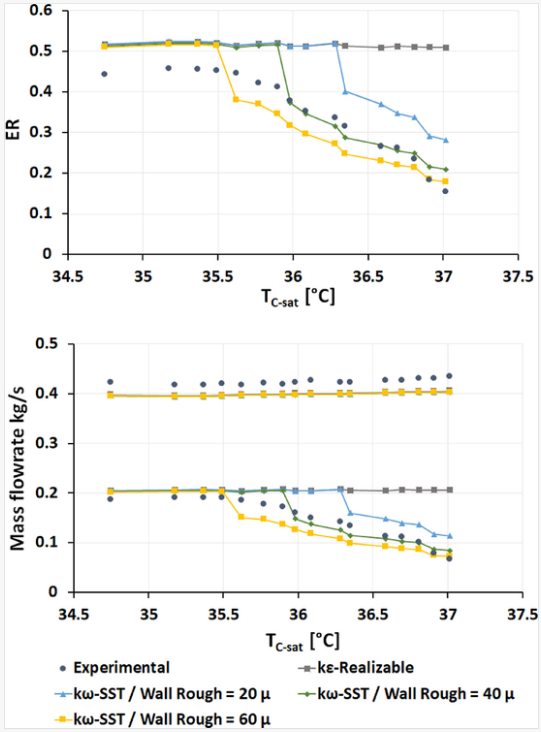

Experimental/numerical comparison Entrainment Ratio, (top) and ejector primary (upper curve of the bottom graph) and secondary (lower curve of the bottom graph) mass flow rate for different values of simulated wall roughness; T_G = 103°C, $T_{E\text{-}sat}$ = 10°C.

The differences in the predicted entrainment ratios are around 15% at on design conditions. Clearly, all the numerical models show the same trend, and differences between various models and roughness heights are negligible in on-design (choked) conditions.

On the other hand, the bottom graph shows that the error appears much lower when the mass flow rates are compared separately and they reach average values of 5.7% and 7.3% for the primary and secondary mass flow rates respectively. This effect is due to summation of the two errors, caused by the fact that CFD underestimates the primary flow rate while, at the same time, it overestimates the secondary mass flow rate.

As the condenser pressure increases, higher values of friction cause the critical state to appear in advance. This result is indeed expected, as greater friction translates into larger amounts of total pressure losses, thus reducing the capability of the mixed flow to withstand high values of backpressure. On the contrary, in the case of smooth surfaces ($k\varepsilon$-Realizable), the simulated ejector maintains choked conditions for higher temperatures at the condenser. This analysis highlights the importance of the manufacturing process on the performance of a supersonic ejector refrigerator, as smoother surfaces imply achieving larger values of critical pressures.

Although the numerical transition to off-design seems steeper than the experiments for any of the CFD models, nevertheless it appears that the $k\omega$-SST method with wall roughness 40μ more closely reproduces the experimental data. At roughness height of 60μ, the transition appears earlier than experiments and the range of "non-choked" operations becomes larger. On the other hand, a lower level of roughness yields higher critical pressure than the experimental one. Therefore, the 40μ roughness is selected for all subsequent calculations.

Indeed, the average roughness height (K_a) of the ejector internal surface was experimentally measured in different locations through a Mahr contact surface profilometer (Mazzelli and Milazzo, 2015). The resulting values of K_a ranged from 4 to 6 microns depending on the different measurement sites. This value of roughness cannot be directly confronted with that obtained from CFD (around 40 microns), because the two values are based on different definitions.

For historical reasons, the roughness definition used in fluid dynamics is the "uniform sand-grain roughness height", K_s. This definition derives from the experiments on friction losses performed by ~~Nikuradse (~~Nikuradse (1937), which were obtained by covering pipe surfaces with a monolayer of uniform sand grains. Subsequently, Moody made use of

Nikuradse's results to derive his chart (Moody, 1944). As a consequence, roughness height is defined as the mean diameter of the sand grains that cover the surface. This value is what is to be input in ANSYS Fluent (ANSYS Inc 2018). However, the "sand-grain" roughness is a completely different quantity from the arithmetic average roughness height (K_a) that is measured by the profilometer. Therefore, a conversion is needed before comparing the two values.

Unfortunately, there is no exact conversion factor to transform a measured average roughness into an equivalent value of uniform sand grain roughness. A recent study from ~~Adams et al. (~~Adams et al. (2012) estimated theoretically the conversion factors and found that roughly $K_s \sim 5.9\ K_a$. By using this conversion factor, it appears that the roughness height predicted by numerical analysis falls somewhat below the range of the experimental data. However, the difference can be acceptable considering the large uncertainty in the conversion factor and the approximation introduced by the numerical and experimental methods.

Fig. 4 shows the comparison of the selected computational model ($k\omega$-SST, wall roughness = 40μ) with all the experimental curves presented in Fig. 2. As the evaporator temperature is decreased, the computed condenser critical temperature gets farther from the experimental one and reaches a difference greater than 1°C (for $T_{E\text{-}sat}$ = 2.5 and 5°C).

alt-text: Fig. 4

~~Figure~~Fig. 4

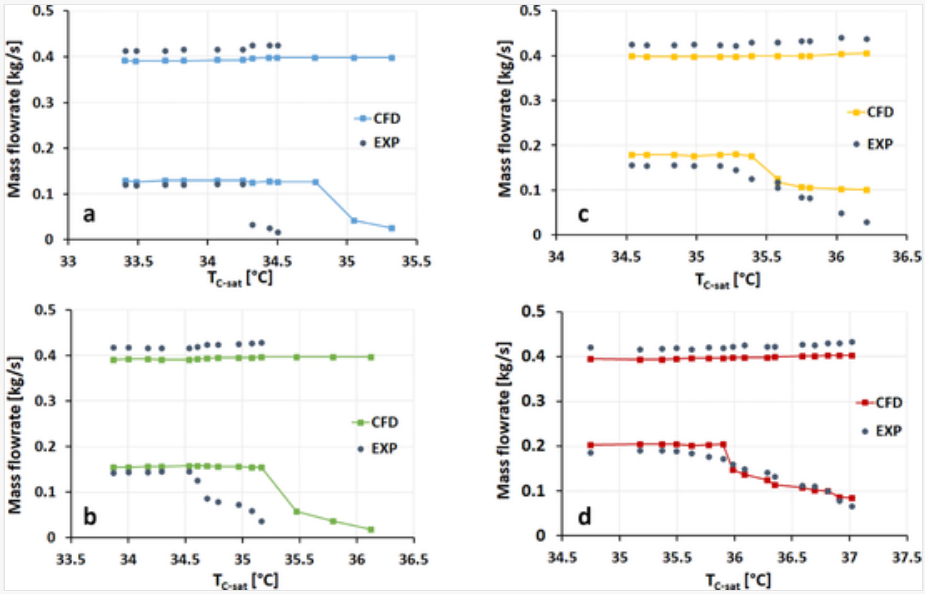

Experimental/numerical comparison of ejector primary (upper curve) and secondary (lower curve) mass flow rate at T_G = 103°C, (a) $T_{E\text{-}sat}$ = 2.5°C, (b) $T_{E\text{-}sat}$ = 5°C, (c) $T_{E\text{-}sat}$ = 7.5°C, (d) $T_{E\text{-}sat}$ = 10°C.

For higher saturation temperatures, the computational trends show a sharper drop at the critical state compared to experiments. At lower temperatures, both the numerical and experimental results show a steeper transition to off-design.

Additional analysis was carried out on the discrepancies between experiments and numerical results, as detailed in the following section.

3.2 Influence of the initialization on CFD simulation results

Fig. 5 shows the comparison between experimental data and CFD results obtained by "moving forward and backward" along the performance curve. We mean by this that the curve labeled "CFD forward" in Fig. 5 was obtained by initializing each CFD simulation from the steady solution of a case with a lower condenser pressure (i.e., at its left in Fig. 5). Conversely, the "CFD backward" curve was obtained by initializing each CFD simulation from the steady solution of a case with a higher condenser pressure (i.e., at its right in Fig. 5). The difference is very evident and may be worth of a discussion.

alt-text: Fig. 5

~~Figure~~Fig. 5

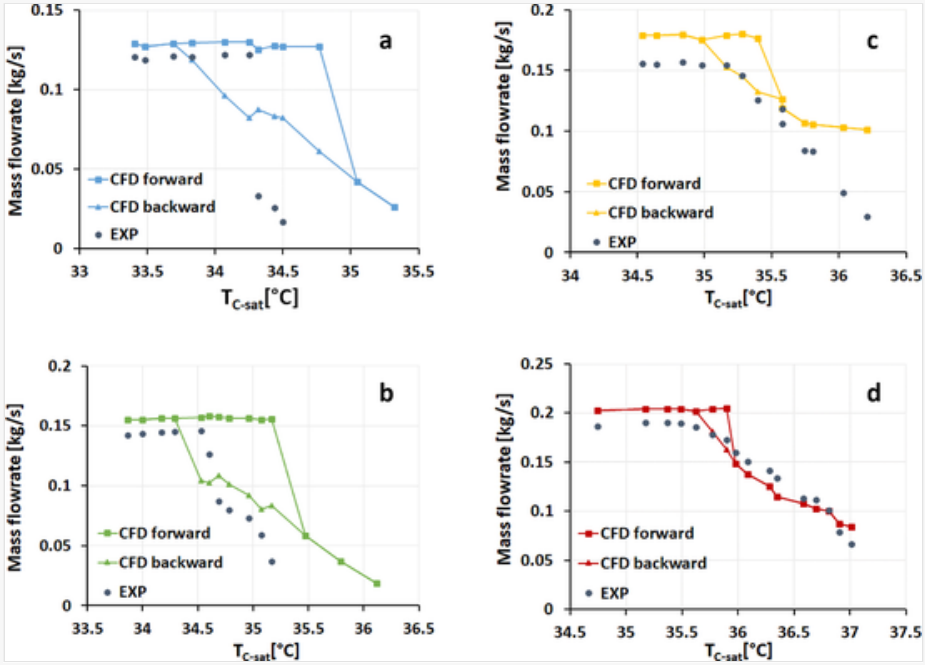

Experimental/numerical (hysteresis) comparison of ejector primary mass flow rate at T_G = 103°C, (a) $T_{E\text{-}sat}$ = 2.5°C, (b) $T_{E\text{-}sat}$ = 5°C, (c) $T_{E\text{-}sat}$ = 7.5°C, (d) $T_{E\text{-}sat}$ = 10°C.

Fig. 5 shows clearly that the critical temperature is anticipated in the backward results and creates a gap with the "CFD forward" curve, i.e., the ejector shows a kind of hysteresis with respect to outlet pressure changes. From Fig. 5 it could be noted that there are two values of pressures that separate the on-design from the off-design regime. The lower of the two is reached by following the backward direction. We may define this value as the "ejector starting pressure". The higher of the two is reached following the forward direction. This is the commonly defined critical pressure, which we may also call the "ejector unstarting pressure". The difference between these two values may be seen as indicative of the presence of hysteresis.

It may be worth clarifying here what we mean by hysteresis. In our interpretation, hysteresis is the phenomenon that causes the final, steady flow solution to be not just dependent on the applied boundary conditions, but also on the history of the previous flow configurations. It is a purely non-linear effect that is caused by the presence of a multistable and multisolution domain (Cui et al., 2011). It is an inherent feature of the system of governing equations that describe the flow; as such, it can be detected and studied using CFD, as testified by numerous publications (Kuzmin, 2018, Shimshi et al., 2009, Mittal, 1998).

Generally, hysteresis loops and bifurcations arise when a critical value of a parameter is exceeded (e.g., angle of attack for supersonic intakes, or critical pressure for supersonic ejectors) and the flow field becomes unstable due to small disturbances. The replacement of the unstable state by a new stable equilibrium state satisfying the same boundary conditions implies failure of the uniqueness condition (Tobak and Chapman, 1985) (which also implies a multisolution and multistable domain). The presence or absence of such small disturbances in the system is an important aspect to consider when discussing discrepancies between the numerical and experimental results. We will resume this aspect later on.

Returning to Fig. 5, the hysteresis loop appears to be wider at lower evaporator temperatures. At 2.5°C evaporation temperature, the difference in the critical pressure between the "CFD backward" and "CFD forward" curves is greater than 15000 Pa (around 1°C in condenser temperature). Moreover, the return to on-design conditions appears to be more gradual than the transition toward off-design conditions (i.e., the forward curve is steeper).

The comparison with experiments shows that the numerical results obtained moving backward appear closer to the experimental data. This is especially true at higher evaporator temperatures, where both the steepness and starting position of the off-design curve is well reproduced by the backward cases. Conversely, at 2.5°C evaporation temperature, the experimental data predict a critical pressure which is between the values of the forward and backward curves. However, the very sudden collapse of the experimental ER appears to be in closer agreement with the forward curve. The error in critical temperature, in this case, is around 0.5°C.

Unfortunately, the experiments do not show evidence of hysteresis, which calls for a deeper discussion of the observed discrepancies.

As a first remark, it should be noted that experiments were carried out before the CFD analyses. Consequently, the tests did not initially involve a "round-trip" loop for the condenser pressure and were generally carried out starting from on-design conditions and progressively increasing the condenser pressure (i.e., moving forward). After the comparison with CFD, additional experiments were conducted to specifically check for the presence of hysteresis, but the tests did not reveal appreciable differences with the original results.

Two possible explanations may exist:

- The discrepancies are caused by differences in the working conditions
- The discrepancies are caused by modeling approximations

The first scenario should not be regarded as simply caused by differences in the value of applied boundary conditions (e.g., the primary pressure is lower in CFD than in experiments). The entire working environment may be responsible for the observed differences, given that experimental tests are subject to multiple disturbances that are absent in the numerical analysis (acoustic, vibrations, pressure fluctuations, jumps in boundary conditions, etc...). From this point of view, the occurrence of metastable flow is possible only if the disturbance intensity is low enough to avoid the transition to a new stable equilibrium state.

By looking at the CFD results, we can even try to quantify the order of magnitude of these oscillations, which should be close to or greater than the difference between the starting and unstarting ejector pressures. In our test, this difference is around 1°C in terms of condenser temperature, i.e., ~6000Pa for the R1233zd(e).

In favor of this thesis, we can report that oscillations of the order of 20 kPa around the average were consistently observed in the primary inlet pressures during the tests. Under this perspective, the absence of hysteresis in experiments may be explained in this terms: as the system moves closer to the critical state (in the forward direction), the oscillation in the primary and secondary pressures may cause the system to jump from the metastable on-design curve (the forward curve in CFD) to the stable off-design curve. This hypothesis may also explain the earlier transition to off-design that is observed in experiments and the closer agreement with the "CFD backward" results.

Unfortunately, a stable working condition with pressure oscillations below said limit is out-of-reach for our experimental set-up. A complete re-design of the system, with different components and advanced control systems would be necessary. Therefore, we will not be able to investigate the problem experimentally in the short term.

Empirical proof that the on-design "forward curve" is a metastable one may come from the discontinuity that is observed at the critical pressure. The passage from on-design to off-design conditions in many ejectors can be abrupt and lead to dramatic changes in the flow fields, e.g., when the shock train at the diffuser is swallowed inside the mixing chamber (as also occurs in supersonic wind tunnels). This behavior is typical of collapsing metastable states, such as during the supersonic and metastable condensation inside steam nozzles and ejectors (Mazzelli et al., 2018).

The second scenario implies that the adopted CFD model has some limitations due to approximations in the numerical discretization, turbulence modeling, axisymmetric domain, etc... Some of these possibilities were tested by sensitivity analyses using different meshes and the cited k-ε turbulence model.

In any case, the difference between "forward" and "backward" CFD results is a problem that deserves further investigation and should be kept in account in the future research on supersonic ejectors.

Herein, we propose a detailed analysis of the flow behavior in the ejector for both the numerical forward and backward cases. This will give further information and insights.

Fig. 6 compares the Mach field between the forward and backward cases for $T_{E\text{-}sat}$ = 10°C. Points a/a′ and d/d′ present the same Mach field for both the forward and backward cases. On the contrary, in points b and c the Mach field for the numerical forward curve displays the diffuser in chocked conditions, while points c′ and d′ in the backward curve show that the ejector operates in the non-chocked or off-design regime. This behavior is even clearer for the case with $T_{E\text{-}sat}$ = 2.5°C illustrated in Fig. 7: points b, c and d show on-design operation in the forward numerical simulations

whereas points b′, c′ and d′ in the backward simulations illustrate off-design condition for the same boundary conditions.

alt-text: Fig. 6

~~Figure~~Fig. 6

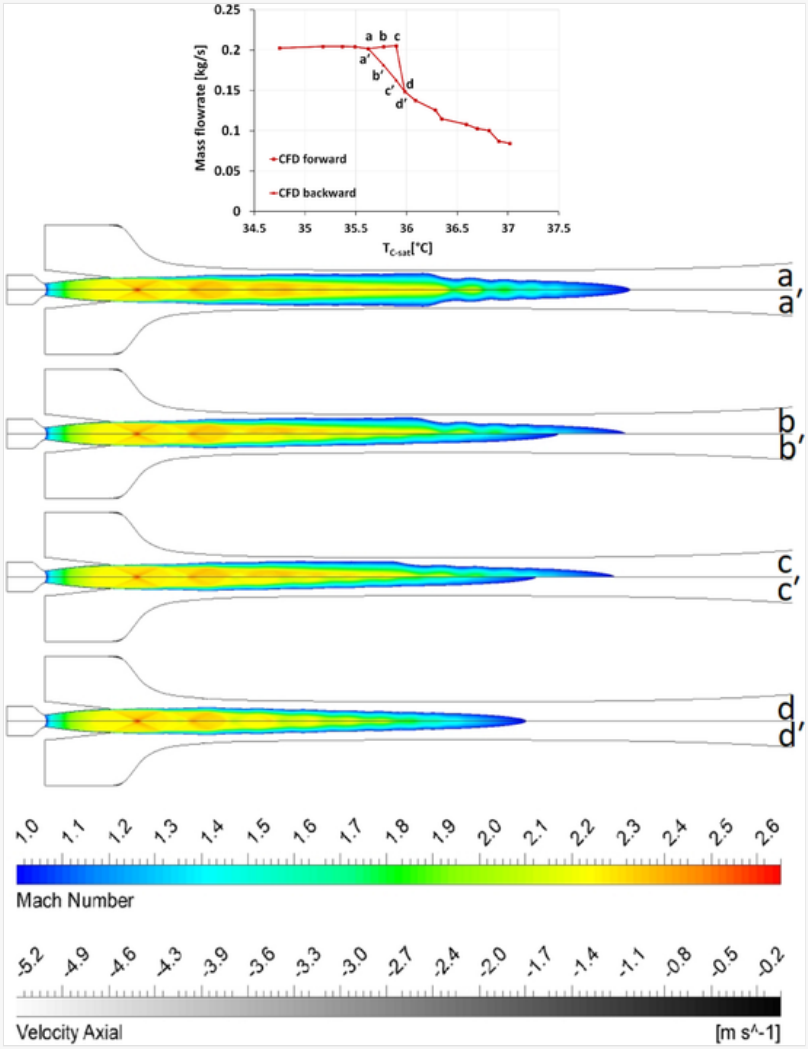

Supersonic Mach field and negative axial velocity (positive direction is from the inlets to the diffuser) along the diffuser at T_G = 103°C, $T_{E\text{-}sat}$ = 10°C for CFD forward (above the axis) and CFD backward (below the axis).

alt-text: Fig. 7

~~Figure~~Fig. 7

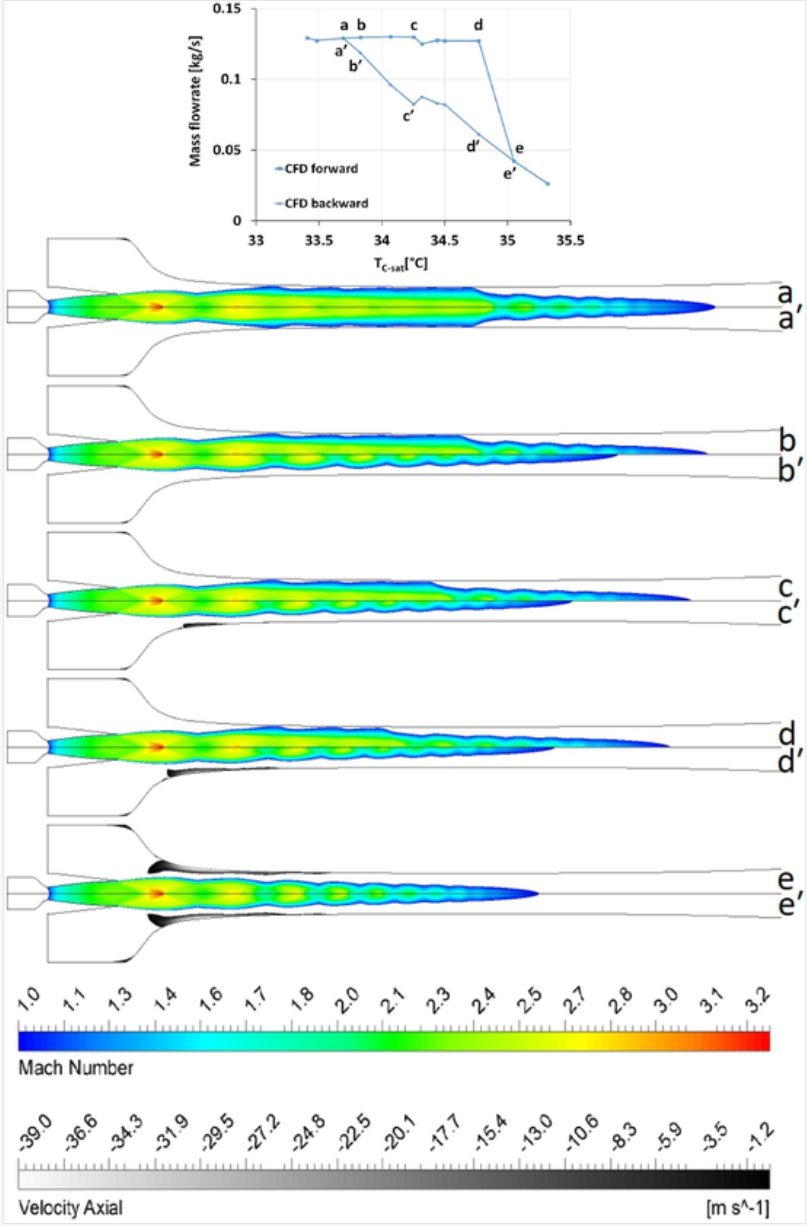

Supersonic Mach field and negative axial velocity (positive direction is from the inlets to the diffuser) along the diffuser at T_G = 103°C, $T_{E\text{-}sat}$ = 2.5°C for CFD forward (above the axis) and CFD backward (below the axis).

A possible reason for the different results between forward and backward simulations can be the presence of the flow recirculation, that is revealed by a negative axial velocity. The contour of axial velocity limited to negative values (in greyscale in the figures) is almost invisible in Fig. 6, apart from a very small area near the ejector inlet, while is quite evident in the low evaporator temperature case (Fig. 7). The increase of condenser pressure in the backward curve creates a recirculation in the convergent area which is evident at state c′ and d′. At point e/e′, the flow behavior is the same for both backward and forward numerical simulations, and both show a strong recirculation in non-chocked conditions. The persistence of a “recirculation-free region” in the forward curve may be viewed as a flow-memory effect caused by the hyperbolic nature of the supersonic flow. In other words, the presence of the sonic line downstream of the ejector's throat may prevent the counter-pressure at the diffuser to influence the flow configuration upstream of the throat, thus retarding the separation of the boundary layer at the inlet of the mixing chamber.

However, recirculation cannot be the sole reason for the inception of hysteresis, as it is practically absent at high evaporator saturation temperature (Fig. 6), but it may be responsible for the hysteresis becoming more persistent when

the evaporation temperature is lower.

3.3 Pressure profile

Fig. 8 shows the comparison between the static pressures measured along the diffuser wall and the corresponding profiles obtained by CFD (kω-SST, wall roughness = 40μ) at T_G = 103°C and $T_{E\text{-}sat}$ = 10°C. In all the graphs, the diffuser throat is located at around 272 mm on the axial direction, between the 4th and 5th pressure transducer.

alt-text: Fig. 8

~~Figure~~Fig. 8

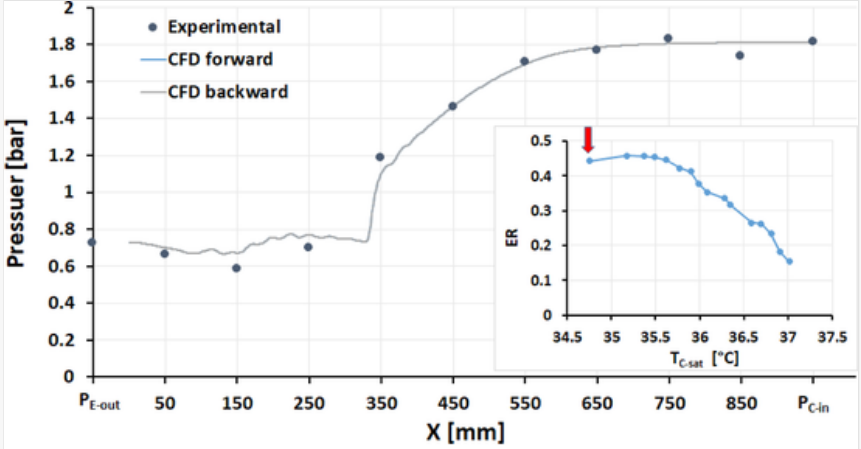
Experimental
CFD forward
CFD backward
Pressuer [bar]
X [mm]
ER
$T_{C\text{-}sat}$ [°C]
$P_{E\text{-}out}$
$P_{C\text{-}in}$

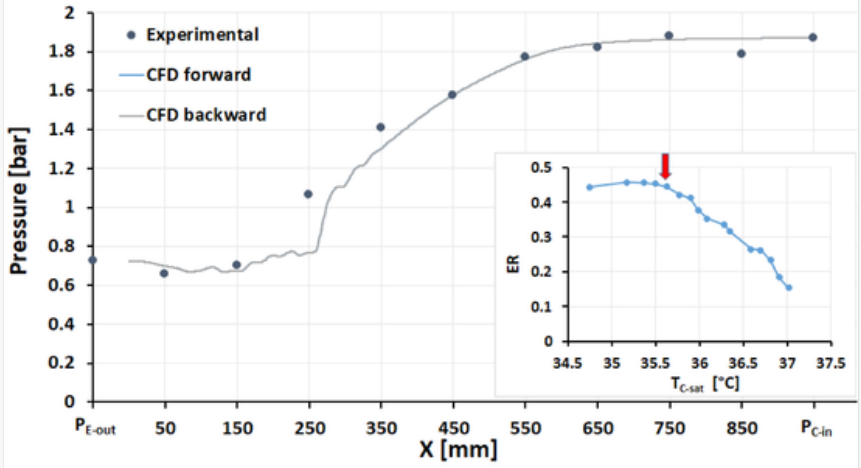
Experimental
CFD forward
CFD backward
Pressure [bar]
X [mm]
ER
$T_{C\text{-}sat}$ [°C]
$P_{E\text{-}out}$
$P_{C\text{-}in}$

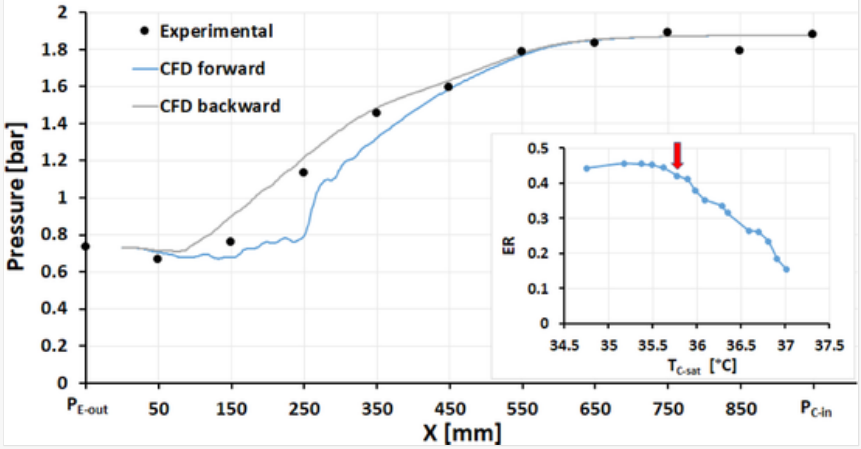
Experimental
CFD forward
CFD backward
Pressure [bar]
X [mm]
ER
$T_{C\text{-}sat}$ [°C]
$P_{E\text{-}out}$
$P_{C\text{-}in}$

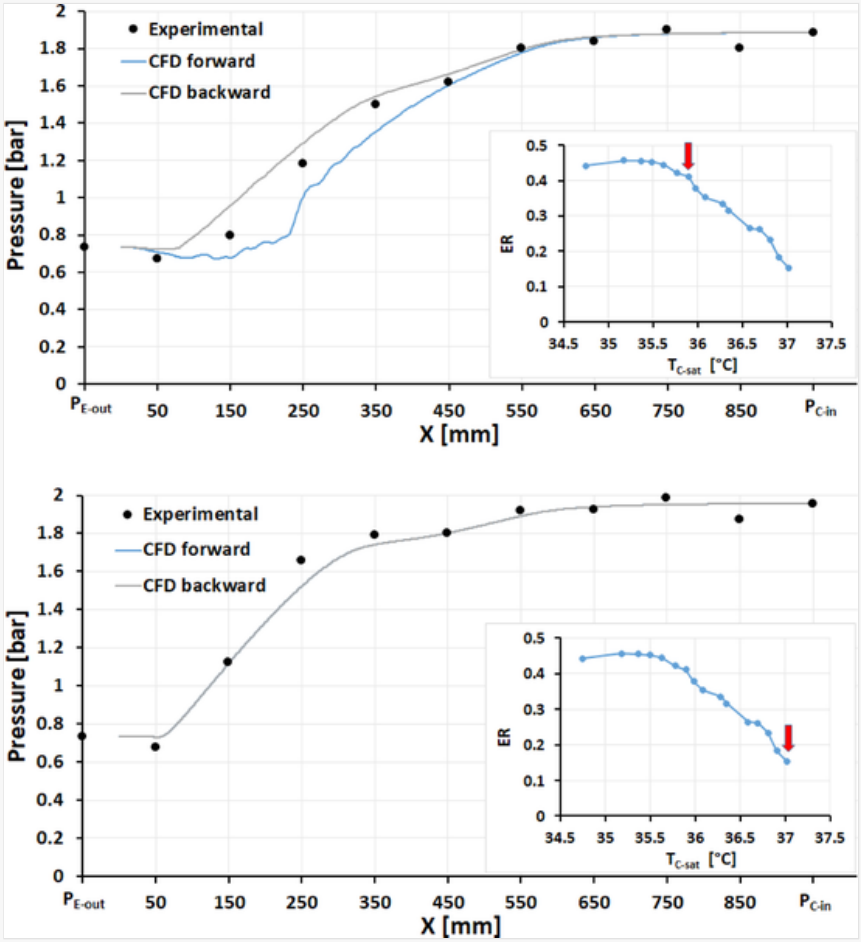

Experimental/numerical comparison of ejector pressure profile at T_G = 103°C, $T_{E\text{-}sat}$ = 10°C. At the bottom/right corner is shown the experimental data point from which the pressure profiles are extrapolated.

The first graph of Fig. 8 shows that the forward and backward simulations are completely overlapping. Pressure fluctuations due to shock diamonds pattern appear before the throat. The sharp rise at around 350 mm from the inlet is indicative of the transition between supersonic and sonic flow, which generally occurs through a shock train (Matsuo et al., 1999). The second graph shows a similar behavior, with a slightly smoother pressure rise that indicates that the shock has moved closer to the diffuser throat (i.e., at lower Mach numbers). In terms of experimental data, the second graph illustrates that the pressure measured by the 4th pressure probe (located at 250 mm) is suddenly increased. This pressure increase occurs before the diffuser throat and indicates that the ejector is not in choked conditions, at least for experimental data. Nevertheless, the ejector can still work with a performance that is almost as good as that at on-design. This smooth transition makes it difficult to understand the jump between chocked and non-chocked diffuser during the experimental test. On the other hand, this behavior is beneficial as the ejector can operate with high performance and in a stable manner even after the inception of off-design conditions.

The on-design conditions are maintained in the third and fourth graphs for the CFD “forward” results, with a slight retraction of the position and strength of the pressure rise. On the other hand, the numerical “backward” result presents a completely different pressure profile, with the pressure increment located between 50 – 100 mm from the inlet, which indicates a complete transition to off-design. The experimental pressure profile falls in the middle of the two numerical pressure profiles. This indicates that while the forward curve underestimates the value of the critical pressure, the backward curve may predict a too-early transition to off-design.

The test at higher condenser pressure reveals that the hysteresis loop has finally closed. The two CFD curves show the same result, which is also very close to experimental tests. A similar trend in pressure profiles occurs under other boundary conditions, not reported for the sake of brevity.

4 Conclusions

This paper presents the computational results obtained from an ejector refrigeration system working with R1233zd(E), whose experimental data were reported in part 1.

The analyses involved the use of different turbulence methods and ejector wall roughness to find the most appropriate numerical setup. Our results indicate that a better agreement between experimental and numerical data can be achieved when the wall roughness is accounted for in the CFD scheme. Wall roughness has not a significant influence on the ER at chocked (on-design) condition. Conversely, friction losses have a large impact on the onset of the non-chocked (off-design) regime, by reducing the critical pressure.

The simulations have revealed that, when the characteristic curve is swept in forward and backward directions (i.e., from lower to higher condenser pressure and vice versa), the transition from off- to the on-design regime takes place at different discharge pressure. This sort of aerodynamic hysteresis is well-known in applications such as supersonic/hypersonic intakes and wind tunnels, but has seldom appeared in studies of supersonic ejectors.

This hysteresis was not evident in the experimental tests of the ejector. Obviously this may be due to simulation problems causing a discrepancy between experimental and CFD results. However, another possible reason for this discrepancy may be the presence of fluctuations in the boundary conditions of the experimental tests. These can drive the system outside a metastable flow configuration and bring it to the new stable equilibrium, thus preventing the appearance of hysteresis.

Under this perspective, the aerodynamic hysteresis in the numerical results may be related to the presence of a multistable and multisolution domain of the non-linear governing equations being solved. Our interpretation is that CFD results, which are not subject to experimental noise and disturbance, can move along a metastable flow configuration (the forward curve) until the critical pressure is reached. From that point on, the system becomes unstable and reaches a new equilibrium flow configuration, i.e., the off-design regime. The return to on-design follows a different and more gradual path that involves reaching a starting pressure, which is lower than the critical pressure. This creates the hysteresis loop.

Moreover, the CFD results show that hysteresis is more significant at lower evaporator temperatures. This could be explained by the appearance of a large separation region close to the suction entrance, which is present in the numerical results that are obtained moving backward, but absent in those obtained moving forward. The hyperbolic nature of the supersonic flow field, which precludes any influence of the outlet pressure on the upstream flow, may contribute to the persistence of this “recirculation-free” region in the forward curve (flow-memory effect). In turn, this may be responsible for the hysteresis becoming wider when the evaporation temperature is lower (i.e, the lower the suction pressure, the higher the recirculation and hysteresis).

Additional experimental campaigns should be designed specifically for detecting any difference between “forward” and “backward” experiments. This requires a highly stable experimental condition when the critical pressure is reached, which is precluded to our present experimental set-up. The resulting data could greatly contribute to the understanding of this complex, but interesting phenomenon.

Declaration of Competing Interest

The authors declare that they have no known competing financial interests or personal relationships that could have appeared to influence the work reported in this paper.

Acknowledgements

The research presented herein has received funding from the MIUR of Italy within the framework of PRIN2015 project «Clean Heating and Cooling Technologies for an Energy-Efficient Smart Grid». A special thanks to Dr. Davide Refosco of Honeywell Performance Materials & Technologies for providing the fluid R1233zd(E).

References

"European Commission," http://ec.europa.eu/clima/policies/f-gas/legislation/index_en.htm., 2017.

Calm, J., 2008. The next generation of refrigerants – Historical review, considerations, and outlook. Int. J. Refrig. 31 (7), 1123–1133.

Calm, J., Hourahan, G., 2011. Physical, safety, and environmental data for current and alternative refrigerants. In: Proceedings of the 23th International Congress of Refrigeration, Prague, Czech Republic.

Fang, Y., Croquer, S., Poncet, S., Aidoun, Z., Bartosiewicz, Y., 2017. Drop-in replacement in a R134 ejector refrigeration cycle by HFO refrigerants. Int. J. Refrig. 77, 87–98.

Milazzo, M., Rocchetti, A., 2015. Modelling of ejector chillers with steam and other working fluids. Int. J. Refrig. 57, 277–287.

Yang, J., Ye, Z., Yu, B., Ouyang, H., Chen, J., 2019. Simultaneous experimental comparison of low GWP refrigerants as drop-in replacements to R245fa for Organic Rankine cycle application: R1234ze(Z), R1233zd(E) and R1336mzz(E). Energy 173, 721–731.

Eyerer, S., Dawo, F., Kaindl, J., Wieland, C., Spliethoff, H., 2019. Experimental investigation of modern ORC working fluids R1224zy(Z) and R1233zd(E) as replacements for R245fa. Appl. Energy J. 240, 946–963.

Mahmoudian, J., Mazzelli, F., Milazzo, A., Rocchetti, A., 2019. Experimental and numerical activity on a prototype ejector chiller. In: Proceedings of the 37th UIT Heat Transfer Conference, Padova.

Matsuo, K., Miyazato, Y., Kim, H., 1999. Shock train and pseudo-shock phenomena in internal gas flows. Progr. Aeros. Sci. 35, 33–100.

Carroll, B., Lopez-Fernandez, P., Dutton, J., 1993. Computations and experiments for a multiple normal shock/boundary-layer interaction. Propul Power 9, 405–411.

Yamane, R., Oshims, S., Nakamura, Y., Ishii, T., Park, M., 1995. Numerical simulation of pseudo-shock in straight channels. JSME Int. J. Series B 38, 549–554.

Pianthong, K., Seehanam, W., Behnia, M., Sriveerakul, T., Aphornratana, S., 2007. Investigation and improvement of ejector refrigeration system using computational fluid dynamics technique. Energy Conv. Manag. 48 (9), 2556–2564.

Mazzelli, F., Little, A.B., Garimella, S., Bartosiewicz, Y., 2015. Computational and experimental analysis of supersonic air ejector: turbulence modeling and assessment of 3D effects. Int. J. Heat Fluid Flow 56, 305–316.

Al-Ansary, H., Jeter, S., 2004. Numerical and experimental analysis of single-phase and two-phase flow in ejectors. HVAC R. Res. 10, 521–538.

Desevaux, P., Aeschbacher, O., 2002. Numerical and experimental flow visualization of the mixing process inside an induced air ejector. Turbo Jet-Engines 19, 71–78.

Zhu, Y., Jiang, P., 2014. Experimental and numerical investigation of the effect of shock wave characteristics on the ejector performance. Int. J. Refrig. 40, 31–42.

Bartosiewicz, Y., Aidoun, Z., Desevaux, P., Mercadier, Y., 2003. CFD/experiments integration in the evaluation of six turbulence models for supersonic ejector modeling. In: Integration CFD and Experiments, Glasgow, UK.

Bartosiewicz, Y., Aidoun, Z., Desevaux, P., Mercadier, Y., 2005. Numerical and experimental investigations on supersonic ejectors. Int. J. Heat Fluid Flow 26, 56–70.

Bartosiewicz, Y., Aidoun, Z., Mercadier, Y., 2006. Numerical assessment of ejector operation for refrigeration applications based on CFD. Appl. Therm. Eng. 26, 604–612.

García del Valle, J., Sierra-Pallares, J., Garcia Carrascal, P., Castro Ruiz, F., 2015. An experimental and computational study of the flow pattern in a refrigerant ejector. Validation of turbulence models and real-gas effects. Appl. Therm. Eng. 1 89 795-81.

Croquer, S., Poncet, S., Aidoun, Z., 2016. Turbulence modeling of a single-phase R134a supersonic ejector. Part1: numerical benchmark. Int. J. Refrig. 61, 140–152.

Aidoun, Z., Ameur, K., Falsafioon, M., Badache, M., 2019. Current advances in ejector modeling, experimentation and applications for refrigeration and heat pumps. part 1: single-phase ejectors. Inventions.

Aidoun, Z., Ameur, K., Falsafioon, M., Badache, M., 2019. Current advances in ejector modeling, experimentation and applications for refrigeration and heat pumps. part 2: two-phase ejectors. Inventions 4 (16), 1–54.

Grazzini, G., Milazzo, A., Mazzelli, F., 2018. Ejectors for Efficient Refrigeration. Springer.

Kim, S., Kwon, S., 2006. Experimental investigation of an annular injection supersonic ejector. AIAA J. 44, 1905–1908.

Kim, S., Kwon, S., 2008. Starting pressure and hysteresis behavior of an annular injection supersonic ejector. AIAA J. 46.

A. Kantrowitz and C. D. Donaldson, "Preliminary Investigation of Supersonic Diffusers," NACA Advance Confidential Report L5D20, 1945.

Pope, A., Goin, K.L., 1965. High-Speed Wind Tunnel Testing. John Wiley & Sons.

Chang, J., Li, N., Xu, K., Bao, W., Yu, D., 2017. Recent research progress on unstart mechanism, detection and control of hypersonic inlet. Progr. Aerosp. Sci. 89, 1–22.

D. M. Van Wie, F. T. Kwok and R.F. Walsh, "Starting characteristics of supersonic inlets," *AIAA Paper*, no. 96-2914, 1996.

Guzhavin, A.I., Korobov, Y.P., 1984. Hysteresis of supersonic flows with separation. Fluid Dyn. 19, 272–280.

Dan'kov, B.N., Kosenko, A.P., Kulikov, V.N., Otmennikov, V.N., 2006. Distinctive features of the transonic flow past a cone-cylinder body at large angles of the bend in the body generator at the leading corner edge. Fluid Dyn. 41, 211–223.

Shimshi, E., Ben-Dor, G., Levy, A., 2009. Viscous simulation of shock-reflection hysteresis in overexpanded planar nozzles. J. Fluid Mech. 635, 189–206.

Mueller, T.J., 1985. The influence of laminar separation and transition on low Reynolds number airfoil hysteresis. J. Aircraft 22 (9), 763–770.

Mittal, S., Saxena, P., 2000. Prediction of hysteresis associated with the static stall of an airfoil. AIAA J. Techn. Notes 38 (5), 933–935.

Liaw, D.-C., Abed, E.H., 1996. Active control of compressor stall inception: a bifurcation-theoretic approach. Automatica 32 (1), 109–115.

Tobak, M., Chapman, G.T., 1985. Nonlinear problems in flight dynamics involving aerodynamic bifurcations. NASA Technical Memorandum 86706.

Holmes, P., Lumley, J., Berkooz, G., Rowley, C., 2012. Turbulence, Coherent Structures, Dynamical Systems and Symmetry. Second ed. Cambridge University Press.

Tao, C., Daren, Y., Juntao, C., Wen, B., 2009. Catastrophe model for supersonic inlet start/unstart. J. Aircraft 46 (4), 1160–1166.

Cui, T., Lv, Z., Yu, D., 2011. Multistability and complex routes of supersonic inlet start/unstart. J. Propulsion Power 27 (6), 1204–1211.

ANSYS Inc, 2018. ANSYS Fluent Theory Guide. Canonsburg, PA release 19.0.

Menter, F., Ferreira, J., Esch, T., Konno, B., 2003. The SST turbulance model with improved wall treatment for heat transfer predictions in gas turbines. In: Proceedings of the International Gas Turbine Congress, Tokyo.

Mazzelli, F., Milazzo, A., 2015. Performance analysis of a supersonic ejector cycle working with R245fa. Int. J. Refrig. 49, 79–92.

Brezgin, D.V., Aronson, K.E., Mazzelli, F., Milazzo, A., 2017. The surface roughness effect on the performance of supersonic ejectors. Thermophys. Aeromech. 24 (4), 569–578.

Nikuradse, J., 1937. Laws of flow in rough pipes. Technical memorandum. NACA.

Moody, L., 1944. Friction factors for pipe flow. ASME Trans. 66.

Adams, T., Grant, C., Watson, H., 2012. A simple algorithm to relate measured surface roughness to equivalent sand-grain roughness. Int. J. Mech. Eng. Mechatron. 1, 66–71.

Kuzmin, A., 2018. Transonic flow hysteresis in a twin intake model. Aeronaut. J. 122, 1557–1567.

Shimshi, E., Ben-Dor, G., Levy, A., 2009. Viscous simulation of shock-reflection hysteresis in overexpanded planar nozzles. J. Fluid Mech. 635, 189–206.

Mittal, S., 1998. Finite element computation of unsteady viscous transonic flows past stationary airfoils. Comput. Mech. 21, 172–188.

Mazzelli, F., Giacomelli, F., Milazzo, A., 2018. CFD modeling of condensing steam ejectors: comparison with an experimental test-case. Int. J. Therm. Sci. 127, 7–18.

Queries and Answers

Q1

Query: Please confirm that givennames and surnames have been identified correctly.

Answer: Yes

Q2

Query: Please validate grant sponsor “MIUR”.

Answer: Yes